Desalination and Water Treatment
www.deswater.com

doi: 10.5004/dwt.2017.21341

89 (2017) 181–188
September

Photocatalytic removal of methyl orange from synthetic wastewater by ternary Fe_3O_4/TiO_2/MWCNTs nanocomposites under visible light

Mohsen Hadipour Bahambar[a], Azadeh Ebrahimian Pirbazari[a,b,*], Neda Gilani[b]

[a]*Caspian Faculty of Engineering, College of Engineering, University of Tehran, P.O. Box 43841-119, Rezvanshahr 43861-56387, Iran, email: mohsen.hadipour@ut.ac.ir (M.H. Bahambar)*
[b]*Fouman Faculty of Engineering, College of Engineering, University of Tehran, P.O. Box 43515-1155, Fouman 43516-66456, Iran, Tel. +981334734927; Fax: +981334737228, emails: aebrahimian@ut.ac.ir (A.E. Pirbazari), gilani@ut.ac.ir (N. Gilani)*

Received 21 April 2017; Accepted 17 August 2017

ABSTRACT

In this work, some hybrids Fe_3O_4/TiO_2/multiwalled carbon nanotubes (MWCNTs; FTC samples) containing different amounts of MWCNTs were synthesized. Then several analyses including X-ray diffractometry (XRD), Fourier transform infrared, scanning electron microscopy (SEM) and energy dispersive X-ray were employed to characterize the crystal structure, morphology and property of the prepared samples. The photocatalytic removal performance of the FTC samples was evaluated by removal of methyl orange (MO) under UV irradiation and visible light. SEM and XRD analyses revealed that TiO_2 NPs with the size of about 11–15 nm and Fe_3O_4 NPs with the size of about 12–45 nm exist in the ternary nanocomposites. The as-synthesized nanocomposites could be rapidly separated from aqueous solutions for repeated use under the external magnetic field. The photocatalytic removal percentage of FTC (0.060) for MO was still 78% after repeating the process for four times.

Keywords: TiO_2; Fe_3O_4; MWCNTs; Photocatalytic removal; Methyl orange

1. Introduction

Photocatalytic degradation by semiconductor nanomaterials especially TiO_2 as a "green technology" has recently attracted attention in water and wastewater treatment, environmental purification and solar energy utilization [1–3]. Titanium oxide (TiO_2) has been widely used in the degradation of different organic and inorganic pollutants for its nontoxicity, high stability, and inexpensiveness [4]. TiO_2 can only be excited by high energy UV irradiation which greatly limits its practical application [5]. Research efforts have focused on integrating TiO_2 with other materials to control electron–hole recombination and increase the limited optical absorption of TiO_2 under sunlight [6–8]. Multiwalled carbon nanotubes (MWCNTs) have been subject of intensive research owing to their unique mechanical, electronic and chemical properties as well as their fascinating one-dimensional tubular structures [9–12]. In the field of aerospace, nanosensor, biology, photocatalyst, and magnetorheological, hybrids consisting of MWCNTs and foreign species are gaining increasing attention in many applications [13–19]. MWCNTs/TiO_2 hybrids have become one of the most commonly mentioned nanomaterials due to their photocatalytic activity in water and wastewater treatment. MWCNTs not only act as an electron transporting bridge to decrease the recombination rate of photogenerated electron–hole pairs and increase photocatalytic activity of the nanocomposite but also act as a support to render the uniform dispersion of TiO_2 and prevent a huge loss of the catalyst [20–24]. However, MWCNTs/TiO_2 hybrids suffer from difficult recollection for environmental applications. Separation by a magnetic field is considered as a quicker and more effective technique than traditional separation technology including centrifugation and filtration as it helps the reduce loss of catalyst to a minimum in the separation of nano-sized materials [25–27]. In the present work, we report the synthesis of ternary Fe_3O_4/TiO_2/carbon nanotube (FTC) samples containing different amounts of MWCNTs. The prepared samples

* Corresponding author.

were characterized by different analyses including, X-ray diffractometry (XRD), Fourier transform infrared (FTIR), scanning electron microscopy (SEM) and energy dispersive X-ray (EDX) techniques. By employing the photocatalytic removal of methyl orange (MO) as a model reaction, we investigated the photocatalytic activity of the prepared nanocomposites. The ternary FTC nanocomposites exhibited an improved durability for successive photocatalytic reactions as compared with the binary Fe_3O_4/TiO_2 nanocomposite.

2. Experimental

2.1. Materials

MWCNTs functionalized by carboxylic groups were provided by Neutrino Corporation (Iran). The average diameter and length of the MWCNTs were 10–20 nm and 0.5–2 μm, respectively. $FeCl_3{\cdot}6H_2O$ (Merck No. 103943) and $FeSO_4{\cdot}7H_2O$ (Merck No. 103965) were used for the synthesis of Fe_3O_4 nanoparticles (NPs). Tetraisopropylorthotitanat (TIP; Merck No. 8.21895), anhydrous ethanol, ammonia, and MO were purchased from Merck. All the reagents were of analytic grade and used without further purification. Double-distilled water was used for the preparation of all aqueous solutions.

2.2. Preparation of Fe_3O_4 NPs

We synthesized Fe_3O_4 NPs by chemical precipitation technique according to mentioned procedure by Laurent et al. [28]. A complete precipitation of Fe_3O_4 was achieved under alkaline conditions, while maintaining a molar ratio of Fe^{2+} to Fe^{3+} 1:2, under an inert environment (nitrogen 99.999%). To obtain 2 g of magnetic particles, 2.1 g of $FeSO_4{\cdot}7H_2O$ and 4.1 g of $FeCl_3{\cdot}6H_2O$ were dissolved in 80 mL of double-distilled water. While the solution was heated to 353 K, 10 mL of aqueous ammonia (25%) was added dropwise to ensure the complete growth of the NP crystals and the solution was heated at 353 K for 30 min. The resulting suspension was cooled to room temperature and then washed three times with 50 mL double-distilled water to remove unreacted chemicals.

2.3. Preparation of Fe_3O_4/TiO_2/MWCNTs samples

In this section, 0.1 g Fe_3O_4 NPs prepared according to abovementioned procedure (section 2.2) and 4 mL tetraisopropylorthotitanat (TIP) were mixed with 70 mL anhydrous ethanol, followed by ultrasonication (ultrasound bath, E60H, ELMA, Germany,) for 1 h. Then, different amounts of functionalized MWCNTs (0.015, 0.030 and 0.060 g) were added to it followed by ultrasonicating it for another 3 h to form solution A. After that, solution B was prepared using 3 mL acetic acid diluted to 90 mL deionized water. Solution B was dropped into solution A at 50°C with mechanical stirring for 30 min. Finally, after cooling to room temperature, the solid product was separated from the suspension by employing a magnet, washed with deionized water and ethanol several times and then dried in a vacuum for 12 h at 60°C. The resulting powder was annealed at 300°C for 1 h to produce Fe_3O_4/TiO_2/MWCNTs nanocomposite. From now on these samples will be shown as FTC (x), where x shows the mass of MWCNTs used during the synthesis. In addition, TiO_2 (T), Fe_3O_4/TiO_2 (FT) and MWCNTs/TiO_2 (CT) samples were synthesized through the same route for control experiments.

2.4. Characterization

FTIR analysis was applied to determine the surface functional groups, using an FTIR-2000, Bruker device, which records the spectra from 4,000 to 400 cm^{-1}. The XRD patterns were recorded on a Siemens, D5000 (Germany). In addition, XRD analysis using an X-ray diffractometer equipped with Cu K_α radiation as the X-ray source. The diffractograms were recorded in the 2θ range of 20°–80°. The morphology of the prepared samples was characterized using SEM (Vega-Tescan) equipped with an EDX.

2.5. Photocatalytic removal of MO

To investigate the photocatalytic removal efficiency of the prepared nanocomposites, the suspension containing 20 mg (optimum dose) nanocomposite and 100 mL aqueous solution of MO (conc. 10 mg/L) was stirred first in the dark for 60 min to establish adsorption/desorption equilibrium. Irradiation experiments were carried out in a self-built reactor and UV illumination was performed with a 400 W Kr lamp (Osram, Germany). The illumination power of the lamp is mainly in the UV-A region, that is, about 90% of the radiated power is in the UV-A region (400–315 nm) and about 10% in the UV-B region (315–280 nm). A visible lamp (500 W, Halogen, Eco Osram) with an emission wavelength ranging from 350 to 800 nm and the predominant peak at 575 nm was used as the irradiation source. At certain intervals, small aliquots (2 mL) were withdrawn and filtered to remove the photocatalyst particles. These aliquots were used for monitoring the removal progress, with Rayleigh UV-2601 UV/VIS spectrophotometer (λ_{max} = 492 nm).

2.6. Statistical analysis

All experiments were performed in triplicate and the average values were presented. The data were analyzed by one-way analysis of variance using SPSS 11.5 for Windows. The data were considered statistically different from control at $P < 0.05$.

3. Results and discussion

3.1. X-ray diffraction analysis

Fig. 1 presents the XRD patterns of the purchased MWCNTs and the synthesized Fe_3O_4 NPs. Fig. 1(a) shows a broad crystalline diffraction around 25.5°, which represents the characteristic diffraction of MWCNTs [29]. In XRD pattern of Fe_3O_4 NPs (Fig. 1(b)), we detected that the characteristic diffractions at 2θ = 30.2°, 35.6°, 43.5°, 54.3°, 57.4°, and 63.1° can be assigned to the reflection of cubic spinel structured of the Fe_3O_4, which is in good agreement with those reported by JCPDS card number 19-0629 [30] indicating phase purity of Fe_3O_4. Moreover, the well-resolved diffraction peaks reveal good crystallinity of Fe_3O_4 NPs. Fig. 2 shows the XRD

patterns of pure TiO_2 and binary nanocomposites (CT and FT). In XRD pattern of pure TiO_2 (Fig. 2(a)), the strong diffractions at 2θ = 25.3°, 37.7°, 48.0°, 53.8°, 55.0°, and 62.6° indexed to pure anatase phase [31]. In the XRD pattern of the sample MWCNTs/TiO_2 (CT), we did not detect any strong and main diffraction of MWCNTs at 25.5° (Fig. 2(b)), which was overlapped with the main diffraction of anatase TiO_2 at 2θ = 25.3°. This observation confirms that the relatively large difference between the mass percents of MWCNTs and TiO_2 could be the reason for the MWCNTs diffraction not to be detectable [32]. In XRD pattern of Fe_3O_4/TiO_2 (FT) sample (Fig. 2(c)), the diffractions became relative weaker than the pure Fe_3O_4 and TiO_2 (Figs. 1 and 2) but matched well with the XRD patterns of TiO_2 and Fe_3O_4 which confirmed that this sample containing Fe_3O_4 and TiO_2 NPs. The diffractions of Fe_3O_4 NPs denoted by an asterisk in Fig. 2(c). Fig. 3 illustrates the XRD patterns of ternary, Fe_3O_4/TiO_2/MWCNTs nanocomposites (FTC samples). The diffractions of these samples matched well with the XRD patterns of pure TiO_2 and Fe_3O_4 NPs, however, they are relatively weaker than those of the pure materials. The main diffraction of MWCNTs is not observed because of the low content of MWCNTs compared with Fe_3O_4 and anatase TiO_2. In addition to diffractions of Fe_3O_4 (showed with an asterisk), there are also other diffraction peaks appearing at 2θ = 25.3°, 37.7°, 48.0°, 53.8°, 55.0°, and 62.6° that are indexed to pure anatase TiO_2 [31]. The diffraction patterns of the prepared samples show considerable line width, indicating small crystal. The average crystal size of magnetic Fe_3O_4 NPs and TiO_2 NPs were calculated using the Scherrer formula for the prepared samples [33].

$$D = K\lambda/\beta \cos\theta \quad (1)$$

where D is the average crystal size of the sample, λ the X-ray wavelength (1.54056 Å), β the full width at half maximum of the diffraction peak (radian), K is a constant 0.89, and θ is the diffraction angle at the peak maximum. Moreover, 2θ = 25.3° and 35.6° were selected for average crystal size calculation of TiO_2 and Fe_3O_4, respectively. The results are summarized in Table 1.

3.2. SEM/EDX analysis

The SEM image of pure MWCNTs (Fig. 4(a)) was highly knotted. The surface of MWCNTs is smooth, whereas the surface of the FTC samples turned rough (Figs. 4(d)–(f)). In SEM images of FTC samples, many nanocrystals with the size of 30–45 nm are seen attached to the surface of carbon nanotubes. According to Scherrer formula (Table 1), the average crystal sizes of Fe_3O_4 and TiO_2 are about 12.23 and 11.24 nm, respectively. These nanocrystals with the size of 30–45 nm may be Fe_3O_4 NPs wrapped by TiO_2 NPs [34,35]. In order to further know the chemical composition of the prepared sample, EDX analysis was performed. Table 2 presents the

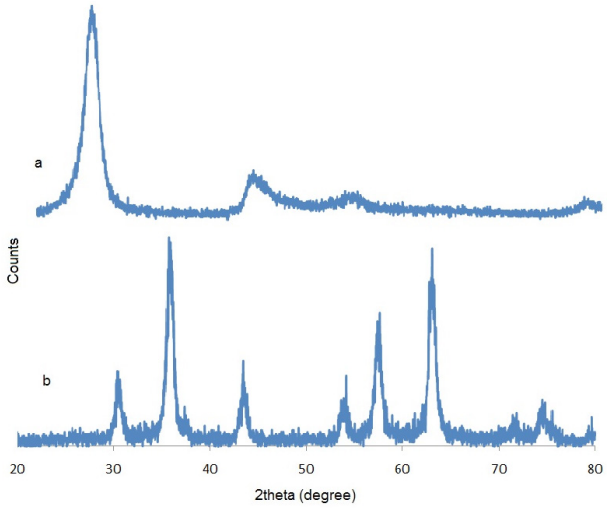

Fig. 1. The XRD patterns of (a) MWCNTS and (b) Fe_3O_4 NPs.

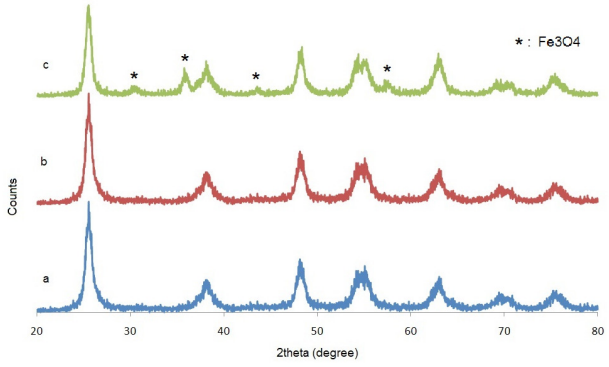

Fig. 2. The XRD patterns of (a) TiO_2, (b) CT and (c) FT.

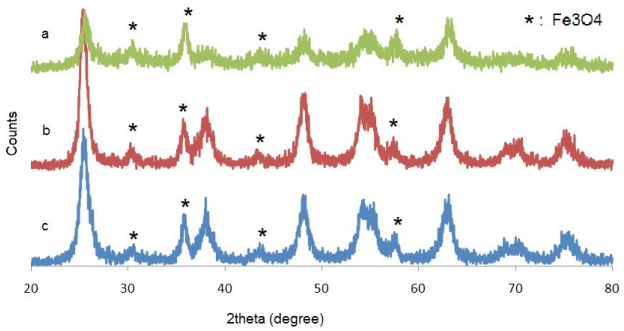

Fig. 3. The XRD patterns of (a) FTC (0.015), (b) FTC (0.030) and (c) FTC (0.060).

Table 1
Average crystal size of the prepared samples according to Scherrer equation

Sample	Fe_3O_4 (nm)	TiO_2 (nm)
Fe_3O_4	12.23	–
TiO_2	–	11.24
CT	–	11.24
FT	22.94	12.58
FTC (0.015)	12.51	15.17
FTC (0.030)	11.52	9.82
FTC (0.060)	12.29	7.74

EDX analysis results for the prepared samples. Using these data, it is revealed that the ternary nanocomposites consist of C, O, Ti, and Fe atoms. In addition, although the existence of carbon atoms is confirmed by EDX analysis but the XRD patterns do not show any diffraction related to MWCNTs. Fig. 5 presents the elemental mapping images of the prepared samples. From the elemental mapping mode, highly and uniformly dispersed Ti and Fe atoms are observed for FTC samples. Accordingly, it is inferred that there is good interaction between Fe_3O_4 and TiO_2 in the preparation process using the sol–gel method.

3.3. FTIR analysis

Fig. 6 shows the FTIR spectra of the prepared samples. In FTIR spectrum of FT sample (Fig. 6(c)), the vibration near 583 cm^{-1} is indexed to the characterized vibrations of Ti–O and Fe–O. Moreover, the vibration at 1,389 cm^{-1} is ascribed to the O–H bond vibration of Ti–OH on the surface of particles. The vibrations at approximately 3,400, 2,930, and 2,850 cm^{-1} are attributed to the Ti–OH bond [36]. The OH bending vibration of chemisorbed and/or physisorbed water molecule on the surface of the catalysts is observed at ~1,630 cm^{-1} for all the samples (Figs. 6(c)–(f)). There are the stretching vibrations of Ti–O–Ti bond in the range of 700–500 cm^{-1} [37].The vibration at 1,515 cm^{-1} is due to the C=C stretching related to the structure of MWCNTs. It is obvious from Fig. 6 that the 500–700 and 1,515 cm^{-1} are corresponding to TiO_2 and MWCNTs, respectively. In FTIR spectrum of CT sample (Fig. 6(d)), the vibration at 1,393 cm^{-1} is indicative of the interaction of COO^- groups on MWCNTs with the titanium dioxide, and the intense broad band in the vicinity of 550 cm^{-1} can be attributed to the combination of Ti–O–Ti and Ti–O–C vibrations between the MWCNTs and TiO_2 [38]. Additionally, the broad vibration in the vicinity of 3,250 cm^{-1} is attributed to not only the presence of hydroxyl groups of TiO_2 but also to a strong interaction through hydrogen bonding between the hydroxyl groups on the surface of titanium dioxide and the carboxyl groups MWCNTs.

3.4. Photocatalytic removal performance of the prepared samples

Fig. 7 shows the performance of the prepared samples for photocatalytic removal of MO under visible light after 120 min irradiation time. As shown in this figure, with increasing the MWCNTs weight, FTC (0.030) and FTC (0.060) samples showed a high photocatalytic removal compared with the other samples. This behavior confirms the role of MWCNTs in these samples: since (1) MWCNTs prevent agglomeration

Table 2
Elemental chemical analysis of the prepared samples

Sample	C wt%	O wt%	Ti wt%	Fe wt%
CT	32.75	34.41	32.84	–
FT	9.85	46.48	39.13	4.54
FTC (0.015)	9.95	56.61	32.20	2.24
FTC (0.030)	11.50	56.17	31.23	1.10
FTC (0.060)	11.56	56.48	30.89	1.06

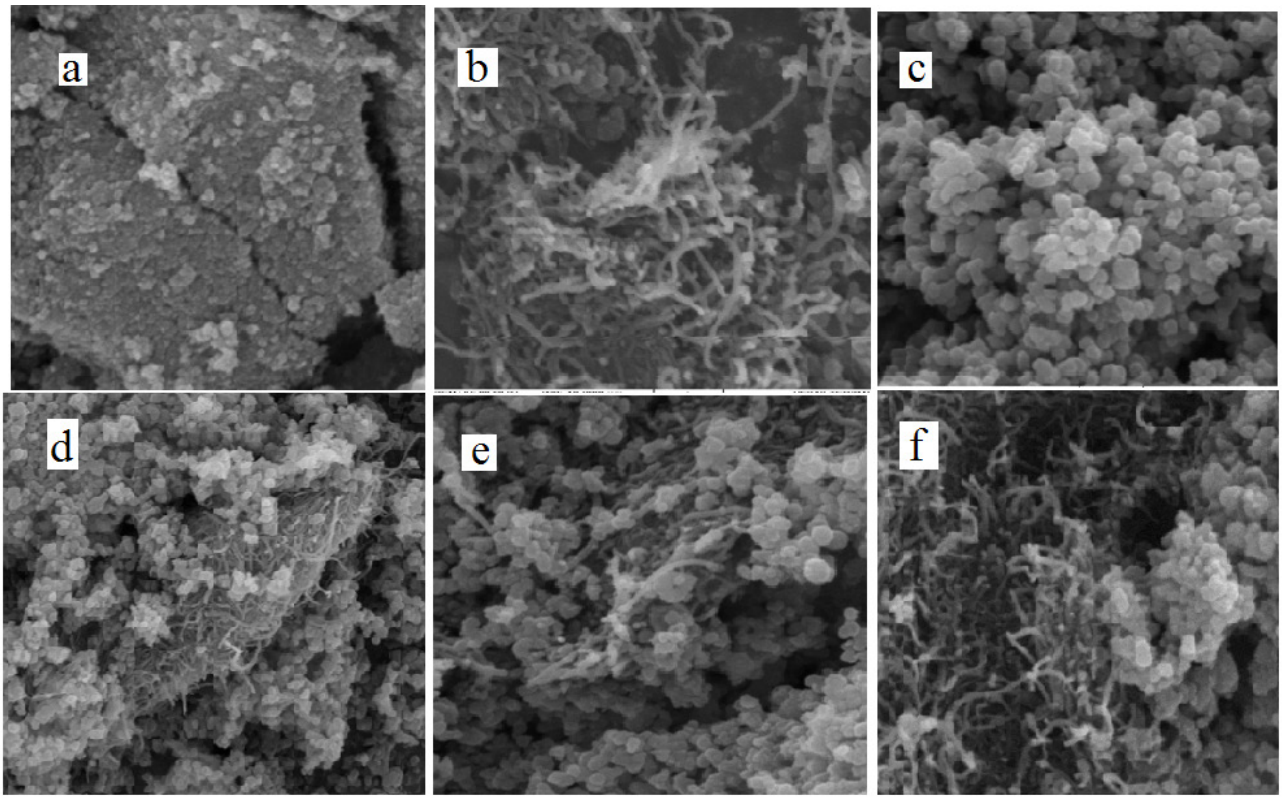

Fig. 4. SEM micrographs of (a) Fe_3O_4, (b) CT, (c) FT, (d) FTC (0.015), (e) FTC (0.030) and (f) FTC (0.060) (SEM Mag = 35,000×, 1 μm).

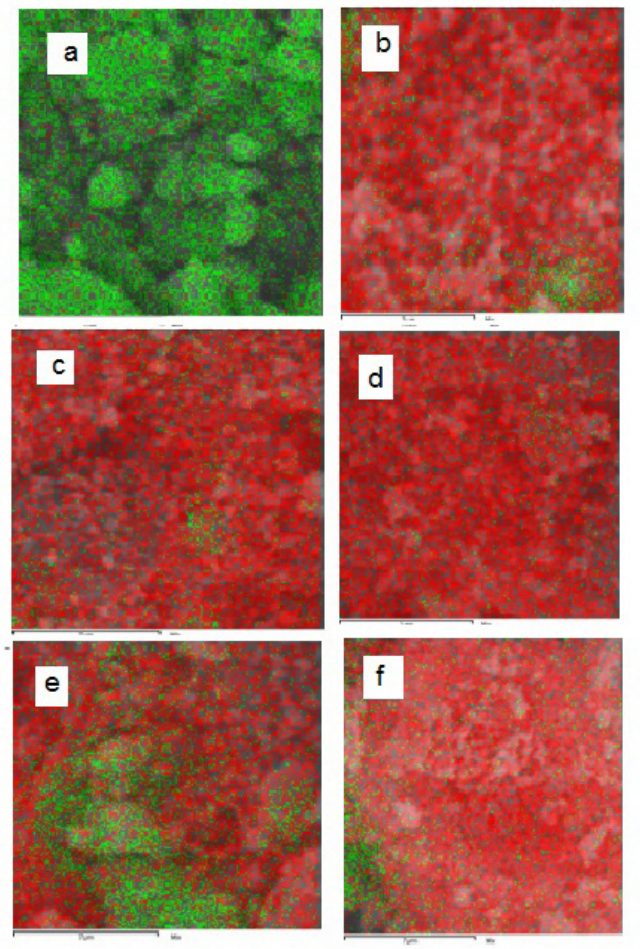

Fig. 5. Elemental mapping images of (a) Fe_3O_4 NPs, (b) FT, (c) CT, (d) FTC (0.015), (e) FTC (0.030) and (f) FTC (0.060).

of TiO_2 by acting as a dispersing agent [32]; (2) In the presence of MWCNTs the adsorption efficiency of FTC samples out performance that of pure TiO_2 because MWCNTs acts as an adsorbent. In addition, MWCNTs in the ternary nanocomposites are useful to adsorb the MO dye and transfer the compound to the surface of TiO_2 (Fig. 8) [39–41]; (3) There is a synergetic effect between MWCNTs and TiO_2 and MWCNTs acting as a photosensitizer. MWCNTs can trap the photoinduced electrons and form superoxide radical ion and/or hydroxyl radical on the surface of TiO_2, which is responsible for the degradation of the organic compound [32,42]. Due to the introduction of the MWCNTs, an increase in the surface charge on TiO_2 in the hybrid catalysts can be suggested. The surface charge may lead to modifications of the fundamental process of electron/hole pair formation while applying visible irradiation [43]. Consequently, it may be the unique interaction between TiO_2 and the MWCNTs that provides the FTC samples with a higher catalytic activity in the photocatalytic removal of MO compared with pure TiO_2.

Fig. 9 shows the photocatalytic removal of MO in the presence of the prepared samples under UV irradiation after 120 min irradiation. The photocatalytic removal efficiency of FTC samples is lower than pure TiO_2 due to the existence of a stronger screen effect in our FTC samples as compared

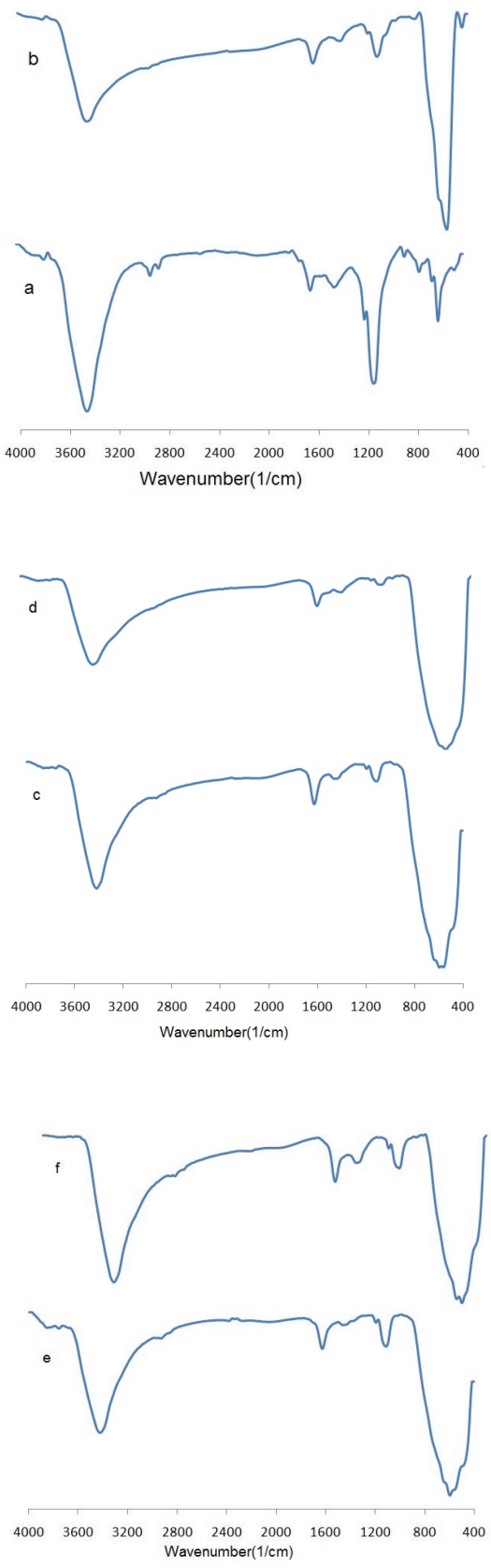

Fig. 6. FTIR spectra of (a) MWCNTs, (b) Fe_3O_4 NPs, (c) FT, (d) CT, (e) FTC (0.030) and (f) FTC (0.060).

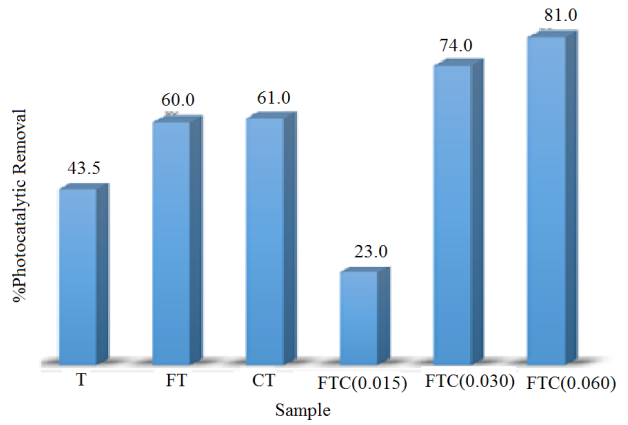

Fig. 7. Photocatalytic removal of MO over the prepared samples (MO conc. 10 mg/L, 20 mg catalyst, 100 mL MO, visible light, irradiation time: 120 min).

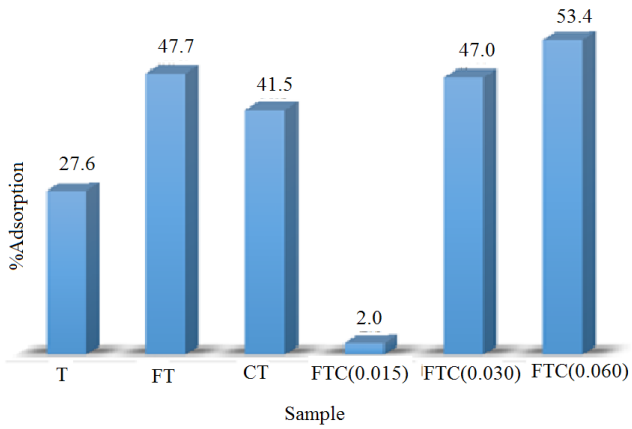

Fig. 8. Adsorption of MO over the prepared samples (MO conc. 10 mg/L, 20 mg catalyst, 100 mL MO, stirring time at dark: 60 min).

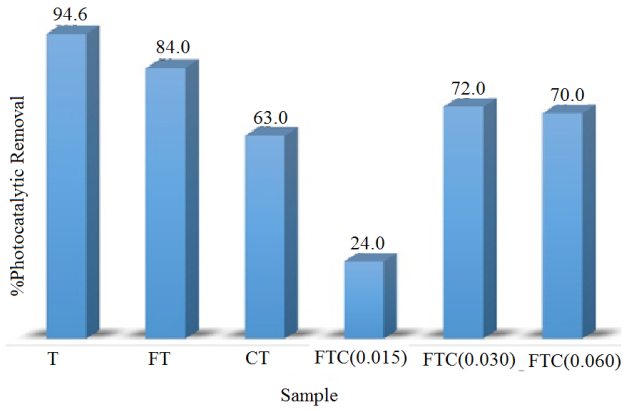

Fig. 9. Photocatalytic removal of MO over the prepared samples (MO conc. 10 mg/L, 20 mg catalyst, 100 mL MO, UV irradiation, irradiation time: 120 min).

with pure TiO_2. The Fe_3O_4 NPs may be screened and thus weaken the UV irradiation needed to irradiate the TiO_2 NPs in the FTC samples [44] because (1) Fe_3O_4 particles blocked some of the TiO_2 active sites and (2) some UV irradiation was absorbed by Fe_3O_4 particles. Accordingly, the photocatalytic removal activity of FTC samples is lower than that of pure TiO_2. The active sites have an important role on the photocatalytic removal activity where charges were generated and/or separated. For more investigation, we prepared FTC samples containing different amounts of MWCNT with fixed amounts of Fe_3O_4 and TiO_2. Our results (Figs. 7 and 9) showed that the introduction of MWCNTs could significantly increase the photocatalytic removal activity of FTC samples. In addition, these results confirmed the proposed mechanism through which MWCNTs act as an acceptor of the electrons generated in the TiO_2 particles, suppress the recombination of charges, and enhance the photocatalytic removal activity of FTC samples [44].

3.5. Reusability of the samples

The reusability of photocatalyst was examined for the removal of MO during a four cycles experiment. The results show that the photocatalytic removal activity of FT sample decrease by 20% after applying these four cycles (from 84% to 62%). The photodissolution of Fe_3O_4 NPs is the main reason for the poor durability of this sample [46]. In the presence of photogenerated electrons, Fe^{3+} in Fe_3O_4 NPs was reduced to $Fe^{2+}$and then dissolved in the solution [45]. For the FTC nanocomposites, the MWCNTs can push most of the photogenerated electrons from the TiO_2 NPs and thus decrease the opportunity of electron transfer to the Fe_3O_4 NPs. TiO_2–Fe_3O_4 binary system, thus enhancing its durability for the photodegradation of MO. To clarify the above discussion, we examined the cyclic photocatalytic removal of the FTC (0.060) sample. No obvious decrease in the photocatalytic removal efficiency (from 81% to 78%) was observed after four cycles, indicating that our FTC sample is renewable for environmental applications.

3.6. The kinetic of MO photocatalytic removal

The photocatalytic removal of MO is a first-order reaction with its kinetics may be expressed as $\ln(C/C_0) = -k_{obs}t$ (Fig. 10). In this equation, k_{obs} (min^{-1}) is the apparent rate constant, C_0 and C are the initial concentration and concentration at reaction time t of MO, respectively. The k_{obs} are found from the slopes of the straight lines obtained by plotting $\ln(C/C_0)$ vs. irradiation time (Fig. 10). The reaction rates, rate constants and half-life ($t_{1/2}$) at various initial concentrations of MO are given in Table 3. The results summarized in Table 3 show that the reaction rate of removal of MO is faster at higher initial concentration. However, the rate constants decrease to some extent when the initial concentration increases.

3.7. The mechanism of photocatalytic removal of MO

The lifetime of the photogenerated electron/hole pairs is the main factor influencing the photocatalytic performance of the prepared samples [46–49]. In the presence of MWCNTs,

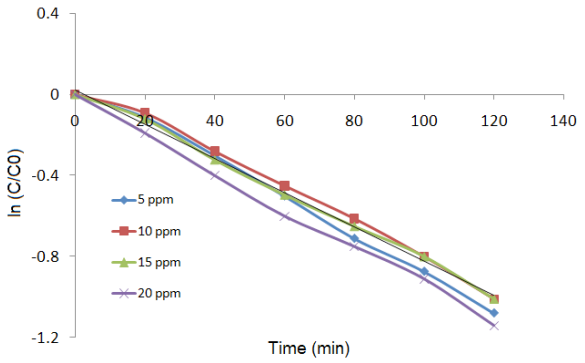

Fig. 10. Effect of initial concentration on the removal of MO. Irradiation. Source: visible lamp, 100 mL MO, 20 mg FTC (0.060).

Table 3
The rate, rate constant (k_{obs}) and half-time ($t_{1/2}$) for various concentrations of MO over FTC (0.060) under visible light

Concentration (mg/L)	R^2	Initial reaction rate (mg/L (min^{-1}))	k_{obs} (min^{-1})	$t_{1/2}$ (min)
5	0.9960	0.046	0.0092	75.34
10	0.9935	0.085	0.0085	81.54
15	0.9933	0.125	0.0083	83.51
20	0.9904	0.162	0.0061	85.57

an effective separation of the photogenerated electron/hole that generated in TiO_2 NPs can be improved. However, its recombination can be suppressed because MWCNTs can store a large number of electrons and transport them. In addition, the crystal size and specific surface area affect the photocatalytic and adsorption ability of the prepared FTC samples. The MWCNTs structure can inhibit the growth of TiO_2 NPs and make reunion phenomenon reduced, which result in the size of TiO_2 NPs decreased in FTC samples (Table 1). The specific surface area and activity can be increased with the decrease in size of TiO_2 NPs. The adsorption ability of samples will be strengthened when the specific surface area is reduced. Such an excellent adsorption ability can increase the contact chance of MO dye molecules, which enhance the photocatalytic removal rate. Therefore, the photocatalytic removal performance was remarkably improved because of the improved efficient separation of the photogenerated electron/hole and the synergic effect between adsorption and photocatalysis process.

4. Conclusion

In summary, ternary Fe_3O_4/TiO_2/MWCNTs nanocomposites containing different amounts of MWCNTs were successfully prepared by the modified sol–gel process and characterized by a different analysis. It was found that the prepared samples present enhanced photocatalytic removal of MO and exhibit expansion in spectral response range shifted to the visible region. This behavior is probably because of the affiliation of some particular properties by MWCNTs support and Fe_3O_4 NPs. The presence of MWCNTs could create many active sites and increase surface area and improve the separation of photogenerated electron–hole pairs. Therefore, adding a suitable amount of MWCNTs into theTiO_2 leads to a great improvement in the photocatalytic removal of MO and thus these samples shows remarkable activity under visible light. The reactions follow a pseudo-first-order kinetics and the observed rate constant values change with MO concentrations. The reusability experiments showed the photocatalytic removal percent of FTC (0.060) for MO is still 78% after repeating the procedure four times.

Acknowledgments

The authors wish to acknowledge the financial support of University of Tehran for supporting of this research.

References

[1] C. Chen, W. Ma, J. Zhao, Semiconductor-mediated photodegradation of pollutants under visible-light irradiation, Chem. Soc. Rev., 39 (2010) 4206–4219.
[2] H. Yin, K. Yu, C. Song, R. Huang, Z. Zhu, Synthesis of Au-decorated V_2O_5@ZnO heteronanostructures and enhanced plasmonic photocatalytic activity, ACS Appl. Mater. Inter., 6 (2014) 14851–14860.
[3] K. Maeda, K. Domen, Photocatalytic water splitting: recent progress and future challenges, J. Phys. Chem. Lett., 1 (2010) 2655–2661.
[4] J.G. Yu, W.G. Wang, B. Cheng, B.L. Su, Enhancement of photocatalytic activity of mesoporous TiO_2 powders by hydrothermal surface fluorination treatment, J. Phys. Chem. C, 113 (2009) 6743–6750.
[5] X. Liu, Z.Q. Liu, S.X. Hao, W. Chu, Facile fabrication of well-dispersed silver nanoparticles loading on TiO_2 nanotube arrays by electrodeposition, Mater. Lett., 80 (2012) 66–68.
[6] Z. Adriana, Doped-TiO_2: A review, Recent Pat. Eng., 2 (2008) 157–164.
[7] M. Pelaeza, T.N.T. Nolan, S.C. Pillai, M.K. Seeryc, P. Falarasd, A.G. Kontosd, P.S.M. Dunlope, J.W.J. Hamiltone, J. A. Byrnee, K. O'Sheaf, M.H. Entezarig, D.D. Dionysioua, A review on the visible light active titanium dioxide photocatalysts for environmental applications, Appl. Catal., B, 125 (2012) 331–349.
[8] S. Mallakpour, E. Khadem, Carbon nanotube–metal oxide nanocomposites: fabrication, properties and applications, Chem. Eng. J., 302 (2016) 344–367.
[9] T. Yamabe, M. Imade, M. Tanaka, T. Sato, Electronic structures and transport properties of carbon nanotube, Synth. Met., 117 (2001) 61–65.
[10] J. Du, L. Zhao, Y. Zeng, L. Zhang, F. Li, P. Liu, C. Liu, Comparison of electrical properties between multi-walled carbon nanotube and graphene nanosheet/high density polyethylene composites with a segregated network structure, Carbon, 49 (2011) 1094–1100.
[11] Q. Cheng, J. Bao, J.G. Park, Z. Liang, C. Zhang, B. Wang, High mechanical performance composite conductor: multi-walled carbon nanotube sheet/bismaleimide nanocomposites, Adv. Funct. Mater., 19 (2009) 3219–3225.
[12] D. Tasis, N. Tagmatarchis, A. Bianco, M. Prato, Chemistry of carbon nanotubes, Chem. Rev., 106 (2006) 1105–1136.
[13] Z. Nan, C. Wei, Q. Yang, Z. Tan, Thermodynamic properties of carbon nanotubes, J. Chem. Eng. Data, 54 (2009) 1367–1370.
[14] P. Diao, Z. Liu, Aligned carbon nanotubes: physics, concepts, fabrication and devices, Adv. Mater., 22 (2010) 1430–1449.
[15] S.W. Ko, M.S. Yang, H.J. Choi, Adsorption of polymer coated magnetite composite particles onto carbon nanotubes and their magnetorheology, Mater. Lett., 63 (2009) 861–863.
[16] J.W. Lee, R. Viswan, Y.J. Choi, Y. Lee, S.Y. Kim, J. Cho, Y. Jo, J.K. Kang, Facile fabrication and superparamagnetism of silica-shielded magnetite nanoparticles on carbon nitride nanotubes, Adv. Funct. Mater., 19 (2009) 2213–2218.

[17] J. Chang, J.H. Lee, C.K. Najeeb, G.H. Nam, M. Lee, J.H. Kim, Area-selective growth of ZnO nanorod arrays on single-walled carbon nanotube patterns, Scr. Mater., 63 (2010) 520–523.
[18] F.F. Fang, H.J. Choi, Y. Seo, Sequential coating of magnetic carbonyliron particles with polystyrene and multiwalled carbon nanotubes and its effect on their magnetorheology, ACS Appl. Mater. Inter., 2 (2010) 54–60.
[19] B.O. Park, B.J. Park, M.J. Hato, H.J. Choi, Soft magnetic carbonyl iron microsphere dispersed in grease and its rheological characteristics under magnetic field, Colloid Polym. Sci., 289 (2010) 381–386.
[20] Y. Dong, D. Tang, C. Li, Special issue: the route to post-Si CMOS devices: from high mobility channels to graphene-like 2D nanosheets, Appl. Surf. Sci., 296 (2014) 1–7.
[21] T. An, J. Chen, X. Nie, G. Li, H. Zhang, X. Liu, H. Zhao, Synthesis of carbon nanotube–nnatase TiO_2 sub-micrometer-sized sphere composite photocatalyst for synergistic degradation of gaseous styrene, ACS Appl. Mater. Inter., 4 (2012) 5988–5996.
[22] H. Wang, S. Dong, Y. Chang, J.L. Faria, Enhancing the photocatalytic properties of TiO_2 by coupling with carbon nanotubes and supporting gold, J. Hazard. Mater., 235–236 (2012) 230–236.
[23] Z. Li, B. Gao, G.Z. Chen, R. Mokaya, S. Sotiropoulos, G.L. Puma, Carbon nanotube/titanium dioxide (CNT/TiO_2) core–shell nanocomposites with tailored shell thickness, CNT content and photocatalytic/photoelectrocatalytic properties, Appl. Catal., B, 110 (2011) 50–57.
[24] J.Y. Ahn, J.H. Kim, K.J. Moon, S.D. Park, S.H. Kim, Synergistic effects of the aspect ratio of TiO_2 nanowires and multi-walled carbon nanotube embedment for enhancing photovoltaic performance of dye-sensitized solar cell, Nanoscale, 5 (2013) 6842–6850.
[25] T. Xin, M. Ma, H. Zhang, J. Gu, S. Wang, M. Liu, Q. Zhang, A facile approach for the synthesis of magnetic separable Fe_3O_4@TiO_2, core–shell nanocomposites as highly recyclable photocatalysts, Appl. Surf. Sci., 288 (2014) 51–59.
[26] J. Jing, J. Li, J. Feng, W. Li, W.W. Yu, Photodegradation of quinoline in water over magnetically separable Fe_3O_4/TiO_2 composite photocatalysts, Chem. Eng. J., 219 (2013) 355–360.
[27] K. Mandel, F. Hutter, C. Gellermann, G. Sextl, Reusable superparamagnetic nanocomposite particles for magnetic separation of iron hydroxide precipitates to remove and recover heavy metal ions from aqueous solutions, Sep. Purif. Technol., 109 (2013)144–147.
[28] S. Laurent, D. Forge, M. Port, A. Roch, C. Robic, L. Vander Elst, R.N. Muller, Magnetic iron oxide nanoparticles: synthesis, stabilization, vectorization, physicochemical characterizations, and biological applications, Chem. Rev., 108 (2008) 2064–2110.
[29] B. Ahmmad, Y. Kusumoto, S. Somekawa, M. Ikeda, Carbon nanotubes synergistically enhance photocatalytic activity of TiO_2, Catal. Commun., 9 (2008)1410–1413.
[30] Z. Mo, C. Zhang, R. Guo, S. Meng, J. Zhang, Synthesis of Fe_3O_4 nanoparticles using controlled ammonia vapor diffusion under ultrasonic irradiation, Ind. Chem. Eng. Res., 50 (2011)3534–3539.
[31] J. Lu, M. Wang, C. Deng, X. Zhang, Facile synthesis of Fe_3O_4@ mesoporous TiO_2 microspheres for selective enrichment of phosphopeptides for phosphoproteomics analysis, Talanta, 105 (2013) 20–27.
[32] W. Wang, P. Serp, P. Kalck, Visible light photodegradation of phenol on MWNT-TiO_2 composite catalysts prepared by a modified sol–gel method, J. Mol. Catal., A, 235 (2005) 194–199.
[33] S. Chang, W. Liu, Surface doping is more beneficial than bulk doping to the photocatalytic activity of vanadium-doped TiO_2, Appl. Catal., B, 101 (2011) 333–342.
[34] P. Zhang, Z. Mo, L. Han, X. Zhu, B. Wang, C. Zhang, Preparation and photocatalytic performance of magnetic TiO_2/montmorillonite/Fe_3O_4 nanocomposites, Ind. Chem. Eng. Res., 53 (2014) 8057–8061.
[35] Z. Mo, P. Zhang, D. Zuo, Y. Sun, H. Chen, Synthesis and characterization of polyaniline nanorods/$Ce(OH)_3$–Pr_2O_3/montmorillonite composites through reverse micelle template, Mater. Res. Bull., 43 (2008) 1664–1669.
[36] Y. Wang, Y. Huang, W. Ho, Biomolecule-controlled hydrothermal synthesis of C–N–S-tridoped TiO_2 nanocrystalline photocatalysts for NO removal under simulated solar light irradiation, J. Hazard. Mater., 169 (2009) 77–87.
[37] E. Bae, W. Choi, Highly enhanced photoreductive degradation of perchlorinated compounds on dye-sensitized metal/TiO_2 under visible light, Environ. Sci. Technol., 37 (2003) 147–152.
[38] G. Hu, X. Meng, X. Feng, Y. Ding, S. Zhang, M. Yang, Anatase TiO_2 nanoparticles/carbon nanotubes nanofibers: preparation, characterization and photocatalytic properties, J. Mater. Sci., 42 (2007) 7162–7170.
[39] J. Matos, J. Laine, J.M. Herrmann, Synergy effect in the photocatalytic degradation of phenol on a suspended mixture of titania and activated carbon, Appl. Catal., B, 18 (1998) 281–291.
[40] C.G. Silva, J.L. Faria, Photochemical and photocatalytic degradation of an azo dye in aqueous solution by UV irradiation, J. Photochem. Photobiol. A, 155 (2003) 133–143.
[41] J. Matos, J. Laine, J.M. Herrmann, Effect of the type of activated carbons on the photocatalytic degradation of aqueous organic pollutants by UV-irradiated titania, J. Catal., 200 (2001) 10–20.
[42] Y. Yu, J.C. Yu, J.G. Yu, Y.C. Kwok, Y.K. Che, J.C. Zhao, L. Ding, W.K. Ge, P.K. Wong, Enhancement of photocatalytic activity of mesoporous TiO_2 by using carbon nanotubes, Appl. Catal., A, 289 (2005) 186–196.
[43] J. Sun, M. Iwasa, L. Gao, Q.H. Zhang, Single-walled carbon nanotubes coated with titania nanoparticles, Carbon 42 (2004) 895–899.
[44] Y. Lin, Zh. Geng, H. Cai, L. Ma, J. Chen, J. Zeng, N. Pan, X. Wang, Ternary graphene–TiO_2–Fe_3O_4 nanocomposite as a recollectable photocatalyst with enhanced durability, J. Inorg. Chem., (2012) 4439–4444.
[45] D. Beydoun, R. Amal, G. K. C. Low, S. McEvoy, Novel photocatalyst: titania-coated magnetite activity and photodissolution, J. Phys. Chem., 104 (2000) 4387–4396.
[46] P. Zhang, Z. Mo, L. Han, Y. Wang, G. Zhaoa, Ch. Zhang, Zh. Li, Magnetic recyclable TiO_2/multi-walled carbon nanotube nanocomposite: synthesis, characterization and enhanced photocatalytic activity, J. Mol. Catal., A, 402 (2015) 17–22.
[47] G. Moon, D. Kim, H. Kim, A.D. Bokare, W. Choi, Platinum-like behavior of reduced graphene oxide as a cocatalyst on TiO_2 for the efficient photocatalytic oxidation of arsenite, Environ. Sci. Technol. Lett., 1 (2014) 185–190.
[48] J. Zhan, H. Zhang, G. Zhu, Magnetic photocatalysts of cenospheres coated with Fe_3O_4/TiO_2 core/shell nanoparticles decorated with Ag nanopartilces, Ceram. Int., 40 (2014) 8547–8559.
[49] V.R. Djokić, A.D. Marinković, O. Ersen, P.S. Uskoković, R.D. Petrović, V.R. Radmilović, D.T. Janaćković, The dependence of the photocatalytic activity of TiO_2/carbon nanotubes nanocomposites on the modification of the carbon nanotubes, Ceram. Int., 40 (2014) 4009–4018.